Research Article

optica

Electrical control of nonlinear quantum optics in a nano-photonic waveguide

DOMINIC HALLETT,[1,†] ANDREW P. FOSTER,[1,*,†] DAVID L. HURST,[1] BEN ROYALL,[1] PIETER KOK,[1] EDMUND CLARKE,[2] IGOR E. ITSKEVICH,[3] A. MARK FOX,[1] MAURICE S. SKOLNICK[1] AND LUKE R. WILSON[1]

[1]*Department of Physics and Astronomy, University of Sheffield, Sheffield S3 7RH, UK*
[2]*Department of Electronic and Electrical Engineering, University of Sheffield, Sheffield S1 3JD, UK*
[3]*School of Engineering and Computer Science, University of Hull, Hull HU6 7RX, UK*
**Corresponding author: andrew.foster@sheffield.ac.uk*

Published XX Month XXXX

S1. Photonic crystal waveguide (PhCWG) design

Figure S1 shows a scanning electron microscope image of the device. The PhCWG has a central slow light section (region I). On either side, PhCWG regions II, III and IV have modified lattice parameters to maximise the optical coupling between the PhCWG and the nanobeam waveguides. The nominal device parameters for the PhCWG are shown in Table S1.

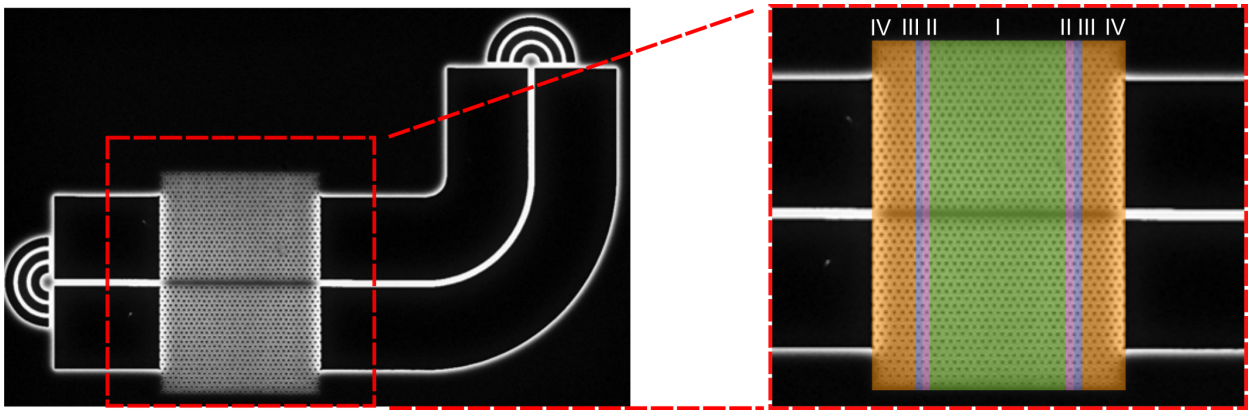

Fig. S1. Scanning electron microscope image of the device. The central section of the photonic crystal (region I, coloured green) is designed with a waveguide band edge at ~900nm. On either side, the photonic crystal parameters are varied (regions II (pink), III (blue) and IV (orange)) to maximise coupling to the nanobeam waveguides.

Table S1. Nominal device parameters for the PhCWG.

	Region I	Region II	Region III	Region IV
Hole radius	82nm			
Hole pitch in x	242nm	1.038x242nm	0.925x242nm	1.06x242nm
Hole pitch in y	242√3nm	242√3nm	242√3nm	242√3nm
Number of lattice periods in x	17	1	1	5
Number of lattice periods in y	24			

S2. Simulated waveguide transmission

Finite difference time domain software (FDTD Solutions, Lumerical Solutions Inc) was used to determine the photonic crystal band edge and transmission through the PhCWG. A broadband mode source was located in one nanobeam waveguide and the transmission measured through the PhCWG by placing a transmission monitor in the second nanobeam waveguide. The results are shown in Fig. S2 for the photonic crystal parameters listed in Table S1, which were used for the device discussed in the main text.

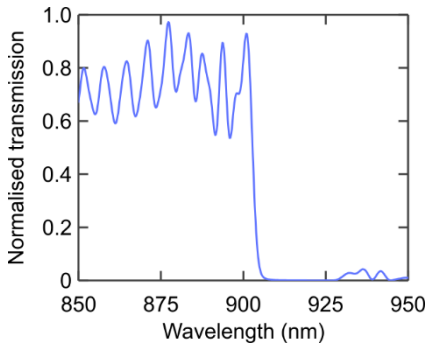

Fig. S2. FDTD simulation of waveguide transmission. Simulated transmission through the photonic crystal waveguide from one nanobeam waveguide to the other.

S3. Cross-correlation of neutral and charged exciton photoluminescence

To demonstrate that the exciton states discussed in the main text originate from the same QD, PL cross-correlation measurements were undertaken. Figure S3a shows the non-resonant PL intensity versus wavelength and bias (also shown in Fig. 1d of the main text) for excitation in the centre of the PhCWG, with three dominant spectral lines visible. Cross-correlation measurements with the X^0 spectral line were performed separately for the spectral lines X^- and X^+. The QD was excited at 808nm with a power of 2.6μW. The voltage applied across the QD was chosen to ensure PL was visible from both of the spectral lines of interest. This was possible because under non-resonant excitation the change of charge state with increasing bias is less abrupt than for resonant excitation (compare for instance Fig. 1d and 2a in the main text). The PL emission was collected from one Bragg grating coupler, split using a 50:50 fiber beam splitter and filtered at the different spectral line wavelengths using separate monochromators. The filtered signals were then detected using two avalanche photodiodes (APDs). The results are shown in Fig. S3 b and c. Cross-correlation of detection events between the two APDs reveal anti-bunching at zero time delay in both cases, indicating that the three emission lines are associated with the same single QD.

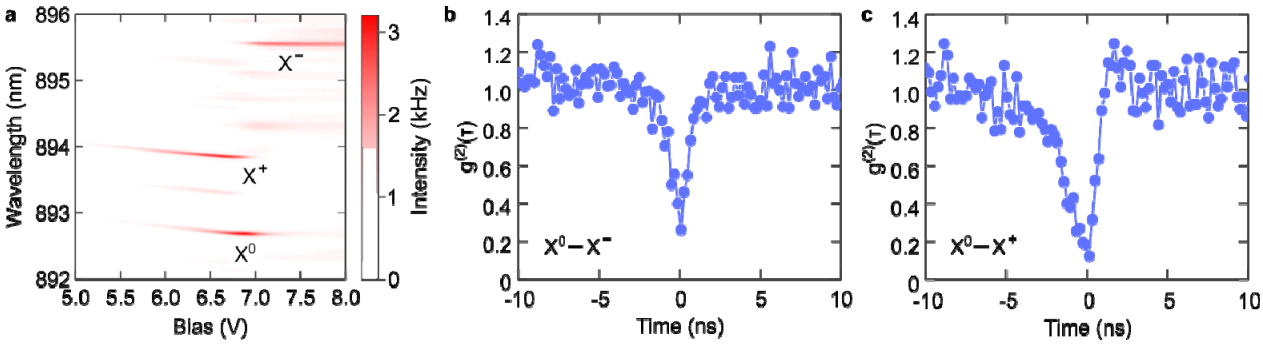

Fig. S3. Cross-correlation measurements between states of the same QD. (a) Non-resonant photoluminescence intensity versus wavelength and bias for a QD located in the photonic crystal waveguide (copy of Fig. 1D of the main text). Cross-correlation of photoluminescence from the X^0 spectral line and the (b) X^- spectral line, (c) X^+ spectral line as shown in (a).

S4. Power dependence of maximum transmission extinction

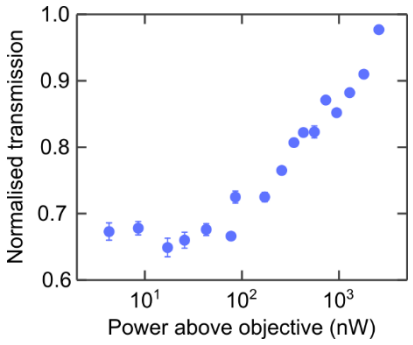

Fig. S4. Power dependence of maximum transmission extinction. The measurement was undertaken on the X_1^0 spectral line at a wavelength of 892.99nm. The bias was swept to vary the X_1^0 -laser detuning and the maximum transmission extinction was then identified for each power.

S5. Nano-photonic device model

Input-Output relations

We consider the system shown schematically in Fig. S5, in which a QD is coupled to the optical mode of a nano-photonic waveguide. If we temporarily neglect dissipative dynamics the corresponding Hamiltonian $H = H_0 + H_{\text{int}}$ is [1]

$$\frac{H_0}{\hbar} = \int \mathrm{d}\varepsilon \left(\omega_0 + \varepsilon\right)\left(r_\varepsilon^\dagger r_\varepsilon + l_\varepsilon^\dagger l_\varepsilon\right) \qquad \frac{H_{\text{int}}}{\hbar} = \frac{1}{2}\Omega\sigma_z + \int \mathrm{d}\varepsilon\left[\left(g_r r_\varepsilon \sigma_+ + g_l l_\varepsilon \sigma_+\right) + \text{H.c.}\right], \tag{S1}$$

where H.c. denotes the Hermitian conjugate of the preceding operator. In the Hamiltonian (S1), r_ε and l_ε are the annihilation operators for right and left-propagating photons of frequency $\omega_0 + \varepsilon$ where ω_0 is the central frequency about which we linearise the waveguide dispersion relation. The frequency of the $|e\rangle \rightarrow |g\rangle$ transition is given by Ω and $g_{r/l}$ represents the coupling amplitude between the emitter and right/left bosonic modes. We have also introduced the Pauli raising and *z* operators, σ_+ and σ_z respectively.

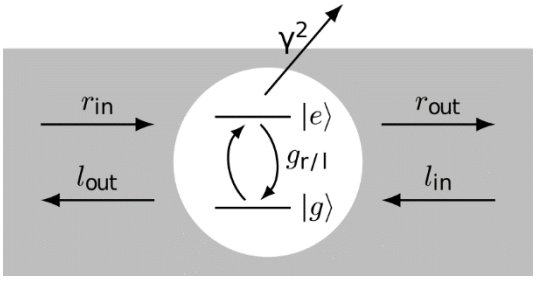

Fig. S5. QD coupling to a single mode nano-photonic waveguide. The QD is modelled as a two level system with ground and excited states $|g\rangle$ and $|e\rangle$ respectively. Annihilation operators for the input optical fields are labelled r_{in} and l_{in} and those for the output fields r_{out} and l_{out}. The QD couples to the right and left propagating optical modes at rates of g_r and g_l respectively, and to non-guided modes at a rate γ^2.

We use the Input-Output formalism of [2] to find the set of coupled differential equations relating annihilation operators for the left and right input fields to the QD dynamics. We further employ the same logic as in [3] to add to the dynamics a finite pure dephasing time τ_{de} and spontaneous emission into unguided modes at a rate proportional to γ^2. Defining the beta factor β as the fraction of photon emission into guided modes and the directional beta factor β_d as the fraction of guided photons emitted into right-propagating modes, we find

$$r_{out} = r_{in} - i\sqrt{\frac{\beta_d \beta}{\tau}}\sigma_- \qquad\qquad l_{out} = l_{in} - i\sqrt{\frac{(1-\beta_d)\beta}{\tau}}\sigma_- \tag{S2}$$

$$\dot{\sigma}_- = -\left(i\Omega + \bar{\gamma}\right)\sigma_- + i\sigma_z\left(\sqrt{\frac{\beta_d \beta}{\tau}}r_{in} + \sqrt{\frac{(1-\beta_d)\beta}{\tau}}l_{in}\right) \tag{S3}$$

$$\text{and} \qquad \dot{N} = -\frac{1}{\tau}N + i\left[\sqrt{\frac{\beta_d \beta}{\tau}}\left(r_{in}^{\dagger}\sigma_- - r_{in}\sigma_+\right) + \sqrt{\frac{(1-\beta_d)\beta}{\tau}}\left(l_{in}^{\dagger}\sigma_- - l_{in}\sigma_+\right)\right], \tag{S4}$$

where $2\bar{\gamma} \equiv 2\gamma_{de} + \gamma + 2\pi g_r^2 + 2\pi g_l^2$ and $N \equiv (\sigma_z + 1)/2$ gives the emitter population. The total lifetime of the emitter, considering all possible decay pathways, is given by τ. Note that τ and β refer to the lifetime and cooperativity of the emitter before the Purcell enhancement is included. For a Purcell factor of F_P we have $\tau \to \tau' = \tau / \left[F_P\beta + (1-\beta)\right]$ and $\beta \to \beta' = F_P\beta / \left[F_P\beta + (1-\beta)\right]$.

In the weak excitation regime it is justifiable to replace the operator σ_z in Eq. (S3) by its average value of -1. If we further assume a coherent input, such that the operators r_{in} and l_{in} are replaced by the complex numbers $re^{-i\omega t}$ and $le^{-i\omega t}$ respectively, then Eq. (S3) can be integrated. We can then substitute the result into Eq. (S2) in order to determine expressions for the output fields in terms of the inputs. If we take the QD as being driven from the left with a coherent field of amplitude r and frequency ω then the transmission spectrum $T(\omega) \equiv \left|\langle r_{out}(\omega)\rangle / \langle r_{in}(\omega)\rangle\right|^2$ is readily determined.

Spectral diffusion and blinking

Charge noise in the QD environment leads to spectral wandering of the exciton energy, characterised here by a variance σ. This means that our previously calculated transmitted intensity $T(\Omega)$ (which is a function of the QD central frequency) must be modified according to

$$T(\Omega) \to T(\Omega, \sigma) = \frac{1}{\sqrt{2\pi\sigma^2}}\int d\varepsilon e^{-\frac{\varepsilon^2}{2\sigma^2}} T(\Omega + \varepsilon) \tag{S5}$$

assuming normally distributed spectral wandering [4]. Furthermore, the QD is not a perfect two-level-system and there is a finite probability P_{dark} that at any given time the QD is in an optically inactive 'dark' state. It is then necessary to make the modification

$$T(\Omega) \to T(\Omega, \sigma, P_{dark}) = (1 - P_{dark})\,T(\Omega, \sigma) + P_{dark}, \tag{S6}$$

where we add P_{dark} to the final result, as having the QD in a dark state corresponds to a transmission of unity (by our normalisation convention).

Fano lineshape

The measured transmission (Fig. 3D of the main text) has a Fano lineshape due to interference between the discrete QD spectral line and the continuum of photonic states arising from Fabry-Perot modes formed by reflection from the Bragg grating couplers (BGCs) and photonic crystal – nanobeam interfaces. Figure S6 shows a schematic for the device including reflection from the aforementioned interfaces. A section of nanobeam waveguide of length d_1 guides light from an input BGC, with reflectivity R_1, to the left end of a PhCWG. The QD is positioned at a distance d_1' from the left hand end of the PhCWG and a distance d_2' from the right hand end, which is connected to a second nanobeam waveguide. This waveguide has length d_2 and is terminated with a BGC which has reflectivity R_2. Reflections at the boundaries between the nanobeam waveguide and PhCWG are denoted by R_1' and R_2'. The presence of reflection means that the lineshape of the calculated

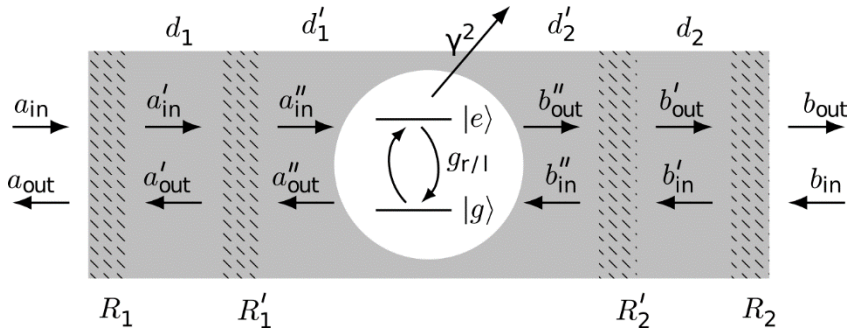

Fig. S6. Schematic of the full nano-photonic device. Annihilation operators for the fields input to the left and right sides of the waveguide are given by a_{in} and b_{in} respectively, and the output fields are a_{out} and b_{out} respectively. Field operators in other sections of the device are given as primed versions of a and b. Reflections at the boundaries of the BGCs and nanobeam waveguides are denoted R_1 and R_2, and those at the nanobeam waveguide – PhCWG boundaries by R_1' and R_2'. The nanobeam waveguides have lengths d_1 and d_2 and the QD is positioned at a distances of d_1' and d_2' from the left and right ends of the PhCWG respectively.

transmission will be sensitive to the position and size of the QD. We therefore model the QD as a rectangular probability distribution in which the $|e\rangle \rightarrow |g\rangle$ transition is located. The probability of finding the exciton at some position x is then described by the probability distribution function

$$p(x) = \begin{cases} \dfrac{1}{L} & x_{cent} - \dfrac{L}{2} \le x \le x_{cent} + \dfrac{L}{2} \\ 0 & \text{otherwise} \end{cases}, \tag{S7}$$

where the QD is centered at position x_{cent} and has a diameter given by L.

In order to quantitatively model the complete system of Fig. S6, we adopt the transfer matrix method presented in [5], assuming each element in the system acts linearly on the input fields. The transfer matrices corresponding to phase-shifting and partially reflecting elements are well known and given in e.g. [6]. We have then eight of the nine transfer matrices required to describe the global system dynamics, corresponding to the four partially-reflecting boundaries and four nano-photonic waveguide regions. The response of the combined system to a given drive field is fully specified by the total transfer matrix, which is a product of the nine matrices corresponding to the individual optical elements. In the weak-excitation regime the output fields of the QD can be expressed as a linear function of the inputs and thus the transfer matrix associated with the QD element can be found by algebraic rearrangement of the input-output relations in Eq. (S2). As a final step, the full calculation is repeated whilst varying the QD position to best match the experimentally observed Fano lineshape.

Table S2 summarises the parameters used in the model and their means of evaluation. The parameters apply to the X_1^0 spectral line. Although the model has several parameters, the majority are known. The position of the QD within the PhCWG is chosen as discussed above to match the experimental lineshape. P_{dark} is then the only unknown parameter which effects the transmission extinction, and is therefore used as a fitting parameter. Note that the variance associated with spectral wandering is calculated from the measured linewidth of 3.7μeV in transmission for the X_1^0 spectral line. The linewidth has Lorentzian and Gaussian contributions arising from the X_1^0 lifetime and spectral wandering respectively. We first calculate the Lorentzian linewidth arising from the radiative transform limit (~1.5μeV for the measured lifetime of 442ps). The linewidth of the Gaussian spectral wandering component is then determined following [7], giving a full width half maximum of 2.8μeV. The is equal to $\sim 2.35\sigma$ and therefore $\sigma = 1.2\mu eV$.

Table S2. Parameters for the transfer matrix model.

Parameter	Symbol	Value	Comments
Spectral line central wavelength	λ_{cent}	892.968 nm	Measured
Lifetime	τ	440 ps	Measured
Pure dephasing time	τ_{de}	2800 ps	Measured
Variance of spectral wandering	σ	1.2 μeV	Measured
Beta factor	β	0.9	Sourced from [8]
Directionality factor	β_{d}	0.5	Asymmetric directional coupling is unlikely in standard PhCWGs [9]
Purcell factor	F_{P}	1.7	Measured
Probability of dark state (blinking)	P_{dark}	0.09	Fitting parameter
QD diameter	L	10 nm	Assumed
Interface reflectivities (see Fig. S6)	R_1 / R_2 R_1' / R_2'	20% / 20% 10% / 10%	Calculated using FDTD
Dimensions (see Fig. S6)	d_1	5 μm	Measured
	d_2	17.9 μm	Measured
	d_1'	5.11 μm	Fitting parameter for Fano lineshape
	d_2'	2.49 μm	Fitting parameter for Fano lineshape. Note $d_1' + d_2' = 7.6\mu\text{m}$ (the length of the PhCWG)

Figure S7a shows the results of the model alongside the experimental data (repeated from Fig. 4a of the main text). A value of $P_{\text{dark}} = 0.09$ is found to be in very good agreement with the data. To demonstrate the potential of this device to realistically generate almost perfect transmission extinction, Fig. S7b shows the increase in transmission extinction that is expected if different QD parameters are improved. Starting with the parameters given in Table S2, we independently set either $\sigma = 0\mu\text{eV}$ or $F_{\text{P}} = 5$. The effect of the increased Purcell factor is of comparable magnitude to the effect of elimination of spectral wandering. We also model a realistically achievable case in which $P_{\text{dark}} = 0$, $F_{\text{P}} = 5$ and $\sigma = 0.2\mu\text{eV}$ (corresponding to a linewidth 20% larger than the transform limit, before accounting for the Purcell enhancement). The transmission extinction in this case is ~95%.

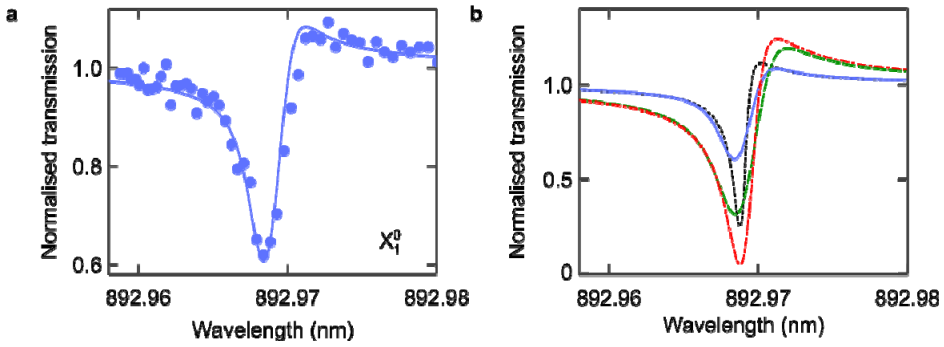

Fig. S7. Calculated device transmission including reflection. (a) Transmission measured for the X_1^0 spectral line (circles). The solid line is the calculated transmission using the parameters given in table S2. (b) Calculated transmission using the parameters in Table S2 (blue solid line) and the same but with $F_P = 5$ (green dashed line), $\sigma = 0\mu eV$ (black dotted line) and $P_{dark} = 0,\ F_P = 5$ and $\sigma = 0.2\mu eV$ simultaneously (red dot-dashed line).

References

1. S. Fan, Ş. E. Kocabaş, and J. T. Shen, "Input-output formalism for few-photon transport in one-dimensional nanophotonic waveguides coupled to a qubit," Phys. Rev. A - At. Mol. Opt. Phys. **82**, 063821 (2010).
2. M. J. Collett and C. W. Gardiner, "Squeezing of intracavity and traveling-wave light fields produced in parametric amplification," Phys. Rev. A **30**, 1386–1391 (1984).
3. A. Auffèves-Garnier, C. Simon, J. M. Gérard, and J. P. Poizat, "Giant optical nonlinearity induced by a single two-level system interacting with a cavity in the Purcell regime," Phys. Rev. A - At. Mol. Opt. Phys. **75**, 053823 (2007).
4. A. Javadi, I. Söllner, M. Arcari, S. L. Hansen, L. Midolo, S. Mahmoodian, G. Kiršanskė, T. Pregnolato, E. H. Lee, J. D. Song, S. Stobbe, and P. Lodahl, "Single-photon non-linear optics with a quantum dot in a waveguide," Nat. Commun. **6**, 8655 (2015).
5. S. Fan, "Sharp asymmetric line shapes in side-coupled waveguide-cavity systems," Appl. Phys. Lett. **80**, 908–910 (2002).
6. J. T. Shen and S. Fan, "Coherent photon transport from spontaneous emission in one-dimensional waveguides.," Opt. Lett. **30**, 2001–3 (2005).
7. J. J. Olivero and R. L. Longbothum, "Empirical fits to the Voigt line width: A brief review," J. Quant. Spectrosc. Radiat. Transf. **17**, 233–236 (1977).
8. M. Arcari, I. Söllner, A. Javadi, S. Lindskov Hansen, S. Mahmoodian, J. Liu, H. Thyrrestrup, E. H. Lee, J. D. Song, S. Stobbe, and P. Lodahl, "Near-Unity Coupling Efficiency of a Quantum Emitter to a Photonic Crystal Waveguide," Phys. Rev. Lett. **113**, 093603 (2014).
9. I. Söllner, S. Mahmoodian, S. L. Hansen, L. Midolo, A. Javadi, G. Kiršanskė, T. Pregnolato, H. El-Ella, E. H. Lee, J. D. Song, S. Stobbe, and P. Lodahl, "Deterministic photon–emitter coupling in chiral photonic circuits," Nat. Nanotechnol. **10**, 775–778 (2015).